



Bis[*N*-(2-hydroxyethyl)-*N*-isopropylthio- carbamato- κ^2S,S'](piperazine- κN)cadmium: crystal structure and Hirshfeld surface analysis

Siti Artikah M. Safbri,^a Siti Nadiyah Abdul Halim,^{a†} Mukesh M. Jotani^b and Edward R. T. Tiekink^{c*}

Received 17 December 2015

Accepted 5 January 2016

Edited by W. T. A. Harrison, University of Aberdeen, Scotland

† Additional correspondence author, e-mail: nadiyahhalim@um.edu.my.

Keywords: crystal structure; Hirshfeld surface analysis; dithiocarbamate; piperazine; hydrogen bonding

CCDC reference: 1445316

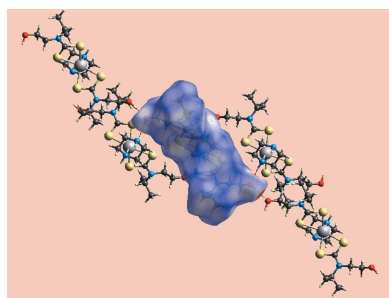
Supporting information: this article has supporting information at journals.iucr.org/e

^aDepartment of Chemistry, University of Malaya, 50603 Kuala Lumpur, Malaysia, ^bDepartment of Physics, Bhavan's Sheth R. A. College of Science, Ahmedabad, Gujarat 380001, India, and ^cCentre for Crystalline Materials, Faculty of Science and Technology, Sunway University, 47500 Bandar Sunway, Selangor Darul Ehsan, Malaysia. *Correspondence e-mail: edwardt@sunway.edu.my

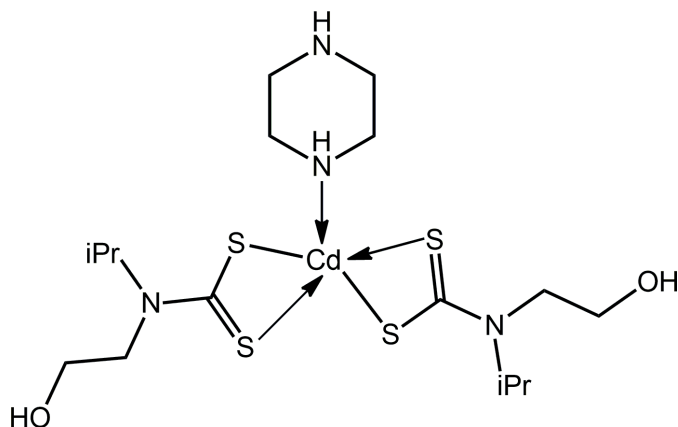
The title compound, [Cd(C₆H₁₂NOS₂)₂(C₄H₁₀N₂)], features a distorted square-pyramidal coordination geometry about the central Cd^{II} atom. The dithiocarbamate ligands are chelating, forming similar Cd–S bond lengths and define the approximate basal plane. One of the N atoms of the piperazine molecule, which adopts a chair conformation, occupies the apical site. In the crystal, supramolecular layers propagating in the *ac* plane are formed *via* hydroxy-O–H···O(hydroxy), hydroxy-O–H···N(terminal-piperazine) and coordinated-piperazine-N–H···O(hydroxy) hydrogen bonds; the layers also feature methine-C–H···S interactions and S···S [3.3714 (10) Å] short contacts. The layers stack along the *b*-axis direction with very weak terminal-piperazine-N–H···O(hydroxy) interactions between them. An evaluation of the Hirshfeld surfaces confirms the importance of intermolecular interactions involving oxygen and sulfur atoms.

1. Chemical context

In the solid state, binary bis(dithiocarbamate) compounds of cadmium are usually binuclear with five-coordinate geometries owing to the presence of equal numbers of chelating and μ_2 -tridentate ligands, *i.e.* are of general formula [Cd(S₂CNR₂)₂]₂ (Tiekink, 2003). Equally well known is the observation that upon the addition of base, this motif is disrupted, resulting in mononuclear species, such as in the case of the pyridine adduct, {Cd[S₂CN(CH₂C(H)Me₂)₂](pyridine)} (Rodina *et al.*, 2011). Ditopic donors can give rise to zero- or one-dimensional species. Thus, when the bidentate ligand is capable of chelating, mononuclear species are obtained, *e.g.* [Cd(S₂CN(Me)^tPr)₂(2,2'-bipyridine)] (Wahab *et al.*, 2011). More variety is found in adducts containing molecules capable of bridging where zero-dimensional binuclear structures, *e.g.* [Cd(S₂CNPr₂)₂(2-pyridinealdazine)]₂ (Poplalkhin & Tiekink, 2008), or supramolecular chains, *e.g.* [Cd(S₂CNET₂)₂(μ_2 -1,2-bis(4-pyridyl)ethylene)]_n (Chai *et al.*, 2003), are found. An intriguing structure has been reported where the potentially μ_2 -bridging ligand, 4-pyridinealdazine, coordinates in the monodentate mode in {Cd[S₂CN(Pr)CH₂CH₂OH]}₂(4-pyridinealdazine)₂ (Broker & Tiekink, 2011). The latter, featuring a dithiocarbamate ligand functionalized with a hydroxyethyl substituent capable of hydrogen bonding, has sparked systematic studies of their wider structural chemistry, revealing hitherto unobserved structural motifs for cadmium dithiocarbamates (Tan *et al.*, 2013, 2016). As a continuation of



this work, the title compound was investigated where both the dithiocarbamate ligand and the nitrogen-donor ligand have hydrogen-bonding potential.



2. Structural commentary

The molecular structure of the title compound, $\{\text{Cd}[\text{S}_2\text{CN}(\text{iPr})\text{CH}_2\text{CH}_2\text{OH}]_2[\text{HN}(\text{CH}_2\text{CH}_2)_2\text{NH}]\}$, Fig. 1, comprises a penta-coordinated cadmium atom, being chelated by two dithiocarbamate ligands and connected to a piperazine-N atom, the latter ligand having a chair conformation. The coordination geometry is best described as being distorted square pyramidal with the nitrogen atom in the apical position. This description is quantified by the value of τ , *i.e.* 0.18, which is closer to the τ value of 0.0 for an ideal square-pyramidal geometry *cf.* 1.0 for an ideal trigonal bipyramid (Addison *et al.*, 1984). The r.m.s. deviation of the four sulfur atoms is 0.1023 Å, and the cadmium atom lies 0.6570 (4) Å above the plane in the direction of the N3 atom. The distortions from the ideal geometry are related, in part, to the acute chelate angles subtended by the chelating ligands, *i.e.* 68–69°, and the range of $\text{N}_{\text{axial}}-\text{Cd}-\text{S}_{\text{basal}}$ angles is 98–116°, Table 1. The dithiocarbamate ligands are coordinating in a slightly

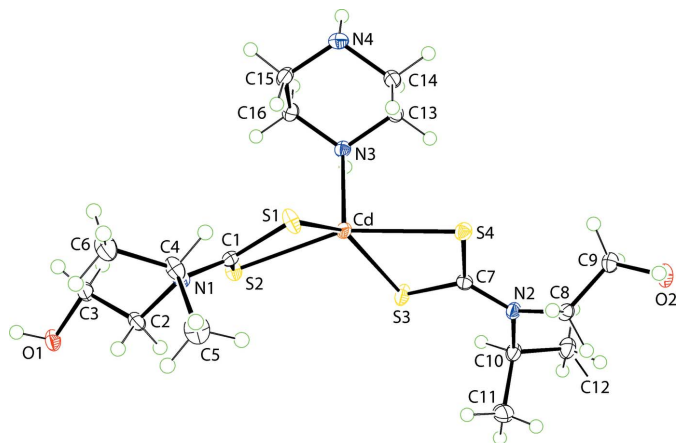


Figure 1

The molecular structure of the title compound, $\{\text{Cd}[\text{S}_2\text{CN}(\text{iPr})\text{CH}_2\text{CH}_2\text{OH}]_2[\text{HN}(\text{CH}_2\text{CH}_2)_2\text{NH}]\}$, showing the atom-labelling scheme and displacement ellipsoids at the 50% probability level.

Table 1

Selected geometric parameters (Å, °).

Cd—S1	2.5503 (6)	C1—S1	1.732 (2)
Cd—S2	2.6580 (8)	C1—S2	1.717 (2)
Cd—S3	2.5446 (6)	C7—S3	1.727 (2)
Cd—S4	2.7461 (8)	C7—S4	1.718 (2)
Cd—N3	2.3102 (17)		
S1—Cd—S2	69.63 (2)	S2—Cd—S4	156.230 (18)
S1—Cd—S3	145.16 (2)	S2—Cd—N3	104.12 (4)
S1—Cd—S4	101.38 (2)	S3—Cd—S4	68.29 (2)
S1—Cd—N3	116.43 (5)	S3—Cd—N3	98.30 (5)
S2—Cd—S3	105.98 (2)	S4—Cd—N3	99.57 (4)

Table 2

Hydrogen-bond geometry (Å, °).

<i>D</i> —H... <i>A</i>	<i>D</i> —H	H... <i>A</i>	<i>D</i> ... <i>A</i>	<i>D</i> —H... <i>A</i>
O1—H1O...O2 ⁱ	0.82 (2)	1.91 (2)	2.673 (2)	155 (2)
O2—H2O...N4 ⁱⁱ	0.83 (2)	1.93 (2)	2.749 (2)	169 (3)
N3—H3N...O1 ⁱⁱⁱ	0.87 (2)	2.05 (2)	2.894 (2)	165 (2)
N4—H4N...O2 ^{iv}	0.87 (1)	2.67 (1)	3.501 (3)	162 (1)
C4—H4...S3 ^v	1.00	2.82	3.641 (3)	140
C10—H10...S1 ^{vi}	1.00	2.83	3.659 (3)	141

Symmetry codes: (i) $x+1, y, z+1$; (ii) $-x+1, -y+1, -z+1$; (iii) $-x+2, -y+1, -z+1$; (iv) $-x+1, y-\frac{1}{2}, -z+\frac{1}{2}$; (v) $x, y, z+1$; (vi) $x, y, z-1$.

asymmetric manner with the difference between the short and long Cd—S bond lengths being *ca.* 0.1 Å for the S1-containing ligand and *ca.* 0.2 Å for the S3-containing ligand, Table 1. The almost symmetric mode of coordination of the dithiocarbamate ligands is reflected in the near equivalence of the associated C—S bond lengths, Table 1, and is consistent with significant delocalization of π -electron density over each four-membered chelate ring.

The monodentate mode of coordination of the piperazine ligand in the title compound is without precedent in the crystallographic literature of cadmium (Groom & Allen, 2014). However, there are several examples of bridging piperazine, *e.g.* $[\text{CdBr}_2(\mu_2\text{-piperazine})]_n$ (Yu *et al.*, 2007), $\{\text{Cd}[1,3\text{-(CO}_2)_2\text{C}_6\text{H}_4](\mu_2\text{-piperazine})(\text{OH}_2)\}_n$ (Gu *et al.*, 2011) and $[\text{Cd}(\text{SCN})_2(\mu_2\text{-piperazine})]_n$ (Suen & Wang, 2007). In common with the title compound, the piperazine ring adopts a chair conformation in each of these structures.

3. Supramolecular features

In the extended structure, hydroxy-O1—H...O2(hydroxy), hydroxy-O2—H...N4(terminal-piperazine) and (coordinated-piperazine)-N3—H...O1(hydroxy) hydrogen bonds (Table 2) lead to the formation of a supramolecular layer in the *ac* plane, Fig. 2. Additional stability to the layers are afforded by methine-C—H...S1, S3 contacts, Table 2, as well as S2...S2ⁱ contacts of 3.3714 (10) Å, for symmetry operation: (i) $2-x, 1-y, 1-z$. Layers thus formed stack along the *b* axis, with very weak terminal-piperazine-N4—H...O2(hydroxy) interactions between them, Table 2 and Fig. 3.

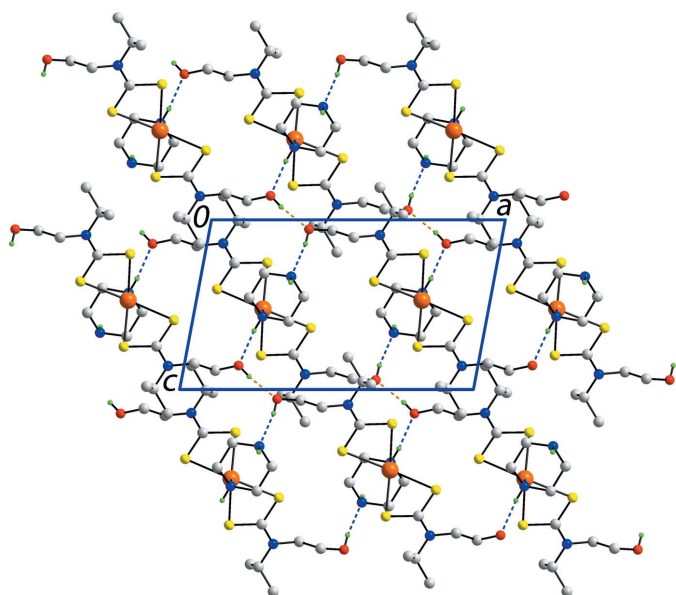


Figure 2
A view of the supramolecular layer in the title compound, shown in projection down the b axis. The hydroxy-O1–H···O2(hydroxy) hydrogen bonds are shown as orange dashed lines while both the hydroxy-O2–H···N4(terminal-piperazine) and (coordinated-piperazine)-N3–H···O1(hydroxy) hydrogen bonds are shown as blue dashed lines. The methine-C–H···S and S···S interactions within the layers (see text) are not shown. Only acidic hydrogen atoms are shown.

4. Analysis of the Hirshfeld surfaces

The program *Crystal Explorer* (Wolff *et al.*, 2012) was used to generate Hirshfeld surfaces mapped over d_{norm} , d_e and electrostatic potential for the title compound. The electrostatic potentials were calculated using *TONTO* (Spackman *et al.*, 2008; Jayatilaka *et al.*, 2005) and were mapped on Hirshfeld surfaces using the STO-3G basis set at the Hartree–Fock level of theory over a range ± 0.14 au. The contact distances d_i and d_e from the Hirshfeld surface to the nearest atom inside and

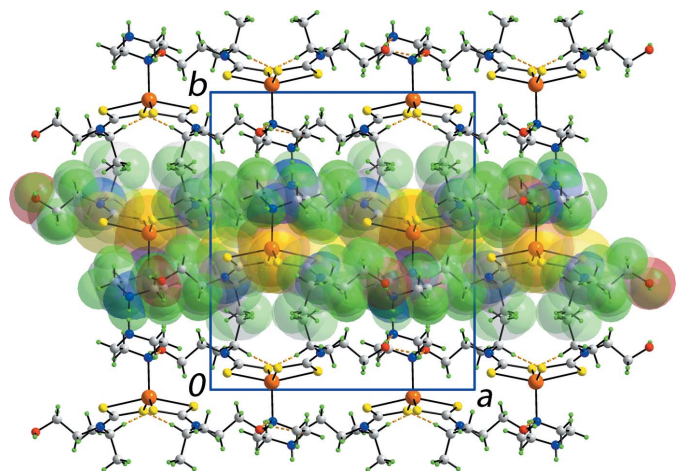


Figure 3
A view of the unit-cell contents of the title compound shown in projection down the c axis, whereby the supramolecular layers, illustrated in Fig. 2, stack along the b axis. One layer is highlighted in space-filling mode.

Table 3
Percentage contribution of the different intermolecular contacts to the Hirshfeld surface.

Contact	Contribution
H···H	67.5
S···H/H···S	17.4
O···H/H···O	7.9
C···H/H···C	3.2
N···H/H···N	2.3
S···S	1.0
Cd···H/H···Cd	0.6
Others	0.1

outside, respectively, enable the analysis of the intermolecular interactions through the mapping of d_{norm} . The combination of d_e and d_i in the form of a two-dimensional fingerprint plot (Rohl *et al.*, 2008) provides a summary of intermolecular contacts in the crystal. The relative contributions from various contacts to the Hirshfeld surfaces are tabulated in Table 3.

The hydrogen-bonding network generated in the crystal through hydroxyl groups located at the edges, piperazine nitrogen-H at the apex and sulfur atoms on the vertices of the distorted square-pyramidal polyhedron can be visualized

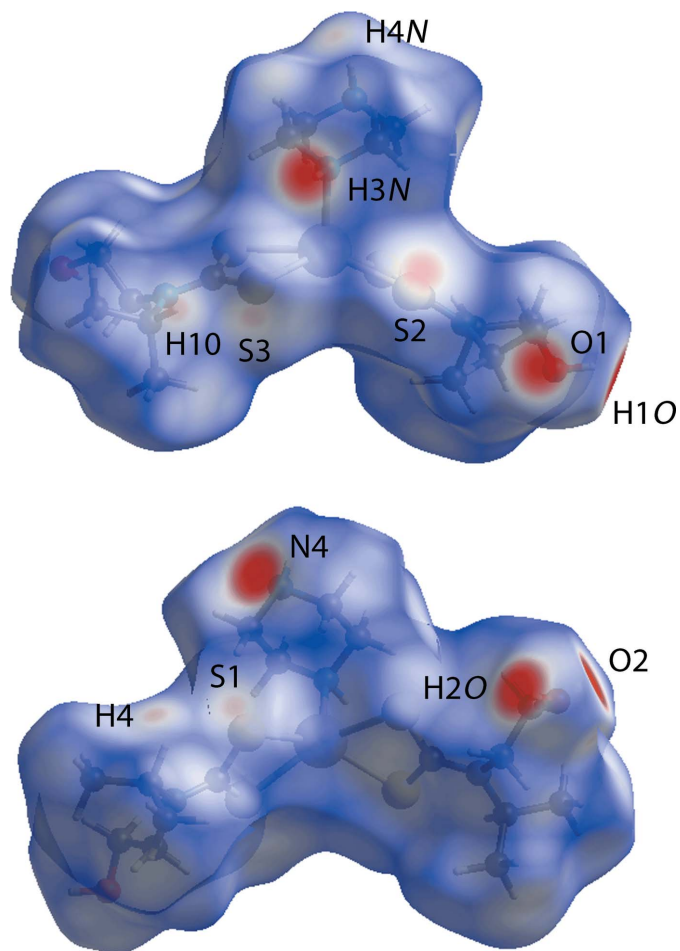


Figure 4
Two views of the Hirshfeld surface mapped over d_{norm} . The contact points (red) are labelled to indicate the atoms participating in the intermolecular interactions.

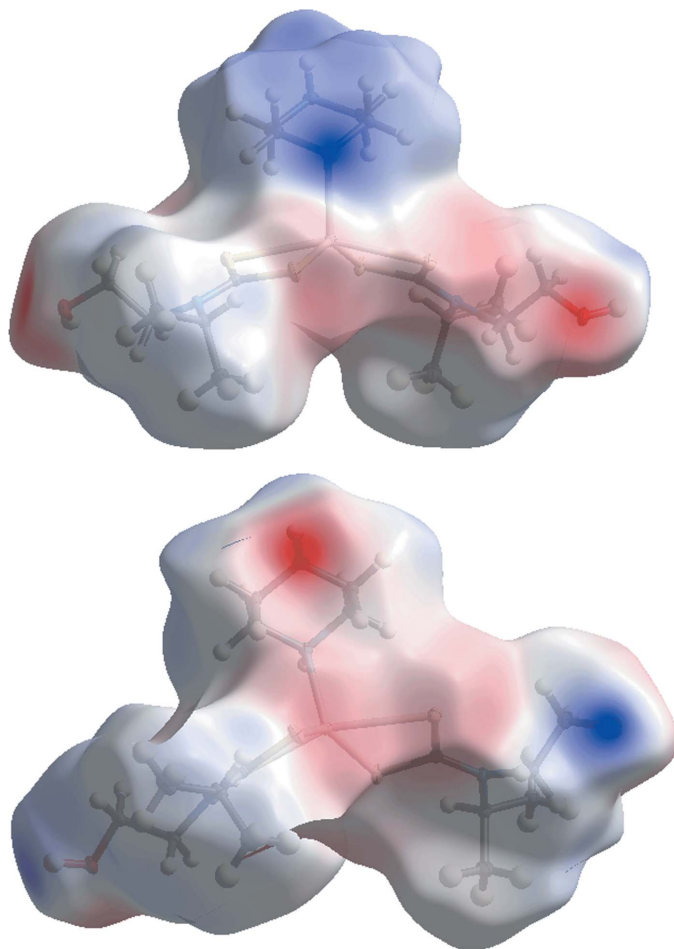


Figure 5
Two views of the Hirshfeld surface mapped over the electrostatic potential with positive and negative potential indicated in blue and red, respectively.

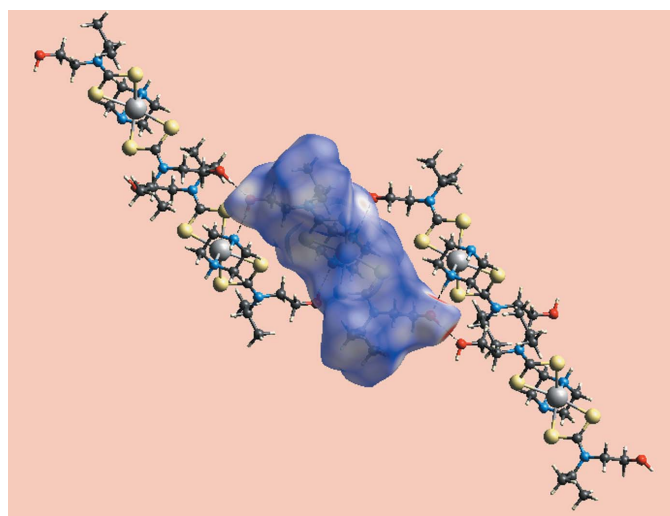


Figure 6
Hirshfeld surface mapped for a reference molecule over d_{norm} showing hydrogen bonds with neighbouring molecules.

using Hirshfeld surface analysis. The bright-red spots on the Hirshfeld surface mapped over d_{norm} , Fig. 4, with labels H1O, H2O and H3N, on the surface represent donors for potential hydrogen bonds, Table 2; the corresponding acceptors on the surfaces appear as bright-red spots at O2, N4 and O1, respectively. The Hirshfeld surface mapped over the electrostatic potential, Fig. 5, represents donors with positive potential (blue regions) and the acceptors with negative potential (red). In addition, the negative potential around the sulfur atoms appear as light-red clouds and the positive potential around piperazine as a light-blue cloud in Fig. 5. The Hirshfeld surfaces mapped over d_{norm} showing intermolecular O—H...O, N—H...O and O—H...N bonds with symmetry-related molecules are shown in Fig. 6. The pale-red depressions near the atoms H4 and S1, and H10 and S3, Fig. 4,

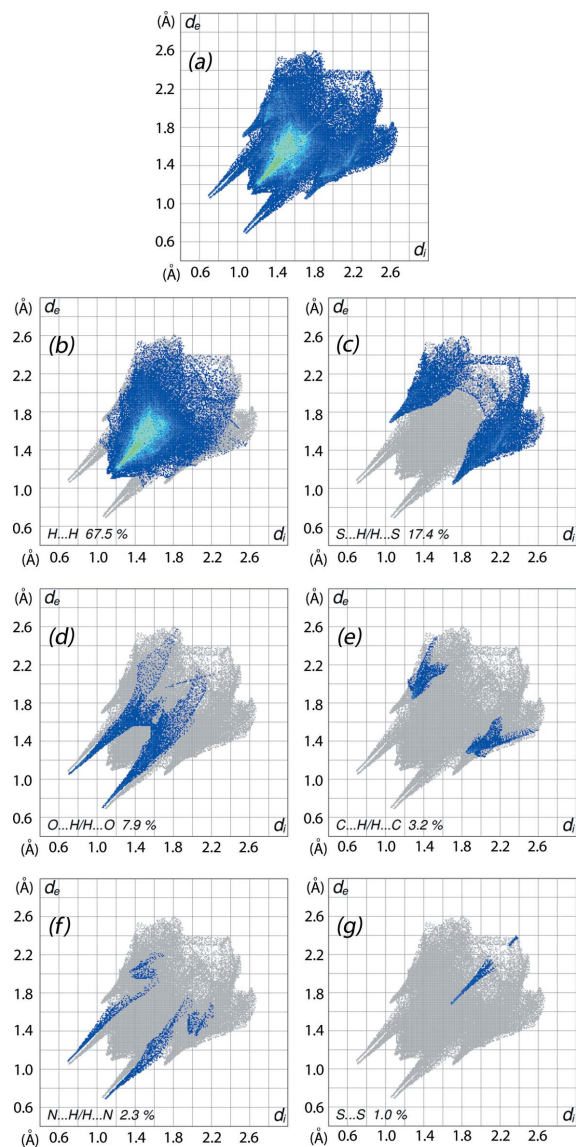


Figure 7
Two-dimensional fingerprint plots: (a) overall, and delineated into contributions from different contacts: (b) H...H, (c) S...H/H...S, (d) O...H/H...O, (e) C...H/H...C, (f) N...H/H...N and (g) S...S.

Table 4
Enrichment ratios (ER).

Contact	ER
H···H	0.98
O···H	1.2
N···H	1.2
C···H	1.2
S···H	1.1
S···S	1.1

confirm the contribution of these pairs of atoms in the comparatively weak intermolecular C—H···S interactions. The pale-red spot near the S2 atom indicates an additional reinforcement to the two-dimensional framework through a non-bonded S···S contact.

The overall two-dimensional fingerprint plot, Fig. 7*a*, and those delineated into H···H, S···H/H···S, O···H/H···O, C···H/H···C, N···H/H···N and S···S interactions are illustrated in Fig. 7*b–g*, respectively. The greatest contribution to the overall Hirshfeld surface, *i.e.* 67.5%, is due to H···H contacts and is reflected in Fig. 4*b* as widely scattered points with a high concentration in the middle region, shown in green. The contribution from the S···H/H···S contacts, corresponding to C—H···S interactions, is represented by the pair of short spikes in the outer region, at $d_e + d_i \sim 2.8 \text{ \AA}$, Fig. 7*c*. In the plots delineated into O···H/H···O and N···H/H···N contacts, Fig. 7*d* and *f*, the pairs of adjacent peaks have almost same lengths near $d_e + d_i \sim 1.8 \text{ \AA}$, and clearly indicate the significance of intermolecular hydrogen bonds associated with them in the molecular packing. There is only a very small contribution from C···H/H···C contacts, *i.e.* 3.2% (Fig. 7*d*), and there is no contribution from C···C contacts in the structure as the result of the absence of C—H··· π and π – π stacking interactions. Finally, the presence of S···S contacts can also be viewed in the delineated fingerprint plot, Fig. 7*g*, by the density of points in the d_e, d_i region around 1.7–2.4 \AA as a broken line segment.

The identified intermolecular interactions were further evaluated by an analysis of the enrichment ratios (ER) that give a quantitative measure of the likelihood of specific intermolecular interactions to occur based on a Hirshfeld surface analysis (Jelsch *et al.*, 2014); ratios are given in Table 4.

A total of 83.2% of the Hirshfeld surface involves hydrogen atoms and of this, non-bonded H···H contacts account for 67.5% of the contacts, which is close to the value of 69.2%, being the value calculated for random contacts so that the corresponding ER value is 0.98, *i.e.* near unity and in accord with earlier published results (Jelsch *et al.*, 2014). The sulfur atoms comprise 9.7% of the surface and S···H/H···S contacts provide an overall 17.4% contribution to the surface resulting in an ER of 1.1 which is in the expected range, *i.e.* 1.0–1.5, for C—H···S interactions. The ER value of 1.2 corresponding to O···H/H···O contacts indicate these show a high propensity to form even though the relative contribution to the overall surface, *i.e.* 7.9%, is small as is the 4.0% exposure to the surface provided by the hydroxyl oxygen atoms. The other contributions to the surface, *i.e.* N···H/H···N and C···H/

Table 5
Experimental details.

Crystal data	
Chemical formula	[Cd(C ₆ H ₁₂ NOS ₂) ₂ (C ₄ H ₁₀ N ₂)
M_r	555.11
Crystal system, space group	Monoclinic, $P2_1/c$
Temperature (K)	100
a, b, c (\AA)	15.341 (3), 16.9915 (7), 9.0308 (8)
β ($^\circ$)	100.620 (16)
V (\AA^3)	2313.7 (5)
Z	4
Radiation type	Mo $K\alpha$
μ (mm^{-1})	1.32
Crystal size (mm)	0.35 \times 0.30 \times 0.25
Data collection	
Diffractometer	Agilent SuperNova Dual diffractometer with Atlas detector
Absorption correction	Multi-scan (<i>CrysAlis PRO</i> ; Agilent, 2011)
T_{\min}, T_{\max}	0.805, 1.000
No. of measured, independent and observed [$I > 2\sigma(I)$] reflections	19918, 5336, 4483
R_{int} ($\sin \theta/\lambda$) _{max} (\AA^{-1})	0.035 0.651
Refinement	
$R[F^2 > 2\sigma(F^2)], wR(F^2), S$	0.026, 0.058, 1.03
No. of reflections	5336
No. of parameters	260
No. of restraints	4
$\Delta\rho_{\text{max}}, \Delta\rho_{\text{min}}$ (e \AA^{-3})	0.45, –0.45

Computer programs: *CrysAlis PRO* (Agilent, 2011), *SHELXS97* (Sheldrick, 2008), *SHELXL2014/7* (Sheldrick, 2015), *ORTEP-3 for Windows* (Farrugia, 2012), *DIAMOND* (Brandenburg, 2006) and *pubCIF* (Westrip, 2010).

H···C, are small and the ER values are not particularly informative although being > 1 , indicate a propensity to form as discussed above in *Supramolecular features*.

5. Database survey

The structural chemistry of cadmium dithiocarbamates where the ligands have been functionalized with one or two hydroxyethyl groups has received some attention in recent years owing to the constant stream of unexpected crystallization outcomes. As mentioned in the *Chemical context*, [Cd(S₂CNR₂)₂]₂ compounds are usually binuclear (Tiekink, 2003). However, recent studies of Cd[S₂CN(^{*i*}Pr)CH₂CH₂OH]₂ (Tan *et al.*, 2013, 2016) have revealed solvent-dependent and solvent-independent supramolecular molecular isomers, *e.g.* crystallization from ethanol produced two species [Cd[S₂CN(^{*i*}Pr)CH₂CH₂OH]₂·EtOH]_{*x*} for $x = 2$ and, unprecedented, n (Tan *et al.*, 2016), with the kinetic, polymeric ($x = n$) form transforming in solution to the thermodynamic, binuclear form ($x = 2$). Other recrystallization conditions led to decomposition of the dithiocarbamate ligands and subsequent formation of a co-crystal and some salts. This behaviour, along with the unexpected structure of {Cd[S₂CN(^{*i*}Pr)CH₂CH₂OH]₂(4-pyridinealdazine)₂} (Broker & Tiekink, 2011) mentioned in the *Chemical context*, suggests this is a fertile area of crystallographic research. Finally, it is noted that gold (Jamaludin *et al.*, 2013), zinc (Tan *et al.*, 2015) and bismuth

(Ishak *et al.*, 2014) compounds of these ligands display promising potential as anti-cancer agents, and that some gold compounds also exhibit exciting anti-microbial activity (Sim *et al.*, 2014).

The monodentate mode of coordination of the piperazine ligand in the title compound is quite rare, and has not been observed in the structural chemistry of cadmium. However, crystallographically confirmed examples of a monodentate coordination mode for piperazine have been seen in five structures, *e.g.* as in centrosymmetric, all-*trans* CoCl₂(piperazine)₂(MeOH)₂ (Suen *et al.*, 2004).

6. Synthesis and crystallization

The reagents Cd[S₂CN^{(i)Pr}CH₂CH₂OH]₂ (Tan *et al.*, 2013; 206 mg, 0.44 mmol) and piperazine (Sigma–Aldrich; 76 mg, 0.43 mmol) were dissolved in chloroform (15 ml) and acetonitrile (5 ml), respectively. The latter solution was added dropwise into the chloroform solution and the resulting mixture was stirred for 1 h at room temperature. Slow evaporation of the clear solution yielded colourless crystals. M.p. 415–417 K. IR (cm⁻¹): ν (O–H) 3281, ν (C–N) 1442, ν (C–O) 1169, ν (C–S) 1029.

7. Refinement

Crystal data, data collection and structure refinement details are summarized in Table 5. The carbon-bound H atoms were placed in calculated positions (C–H = 0.98–1.00 Å) and were included in the refinement in the riding-model approximation, with $U_{\text{iso}}(\text{H})$ set to $1.2U_{\text{eq}}(\text{C})$. The oxygen- and nitrogen-bound H atoms were located in a difference Fourier map but were refined with a distance restraints of O–H = 0.84 ± 0.01 Å and N–H = 0.88 ± 0.01 Å, and with $U_{\text{iso}}(\text{H})$ set to $1.5U_{\text{eq}}(\text{O})$ and $1.2U_{\text{eq}}(\text{N})$.

Acknowledgements

The University of Malaya's Postgraduate Research Grant Scheme (No. PG097-2014B) is gratefully acknowledged.

References

Addison, A. W., Rao, T. N., Reedijk, J., van Rijn, J. & Verschoor, G. C. (1984). *J. Chem. Soc. Dalton Trans.* pp. 1349–1356.
 Agilent (2011). *CrysAlis PRO*. Agilent Technologies Inc., Santa Clara, CA, USA.

Brandenburg, K. (2006). *DIAMOND*. Crystal Impact GbR, Bonn, Germany.
 Broker, G. A. & Tiekink, E. R. T. (2011). *Acta Cryst.* **E67**, m320–m321.
 Chai, J., Lai, C. S., Yan, J. & Tiekink, E. R. T. (2003). *Appl. Organomet. Chem.* **17**, 249–250.
 Farrugia, L. J. (2012). *J. Appl. Cryst.* **45**, 849–854.
 Groom, C. R. & Allen, F. H. (2014). *Angew. Chem. Int. Ed.* **53**, 662–671.
 Gu, J.-Z., Lv, D.-Y., Gao, Z.-Q., Liu, J.-Z., Dou, W. & Tang, Y. (2011). *J. Solid State Chem.* **184**, 675–683.
 Ishak, D. H. A., Ooi, K. K., Ang, K. P., Akim, A. Md., Cheah, Y. K., Nordin, N., Halim, S. N. B. A., Seng, H.-L. & Tiekink, E. R. T. (2014). *J. Inorg. Biochem.* **130**, 38–51.
 Jamaludin, N. S., Goh, Z.-J., Cheah, Y. K., Ang, K.-P., Sim, J. H., Khoo, C. H., Fairuz, Z. A., Halim, S. N. B. A., Ng, S. W., Seng, H.-L. & Tiekink, E. R. T. (2013). *Eur. J. Med. Chem.* **67**, 127–141.
 Jayatilaka, D., Grimwood, D. J., Lee, A., Lemay, A., Russel, A. J., Taylor, C., Wolff, S. K., Cassam-Chenai, P. & Whitton, A. (2005). *TONTO – A System for Computational Chemistry*. Available at: <http://hirshfeldsurface.net/>
 Jelsch, C., Ejsmont, K. & Huder, L. (2014). *IUCrJ*, **1**, 119–128.
 Poplaukhin, P. & Tiekink, E. R. T. (2008). *Acta Cryst.* **E64**, m1176.
 Rodina, T. A., Ivanov, A. V., Gerasimenko, A. V., Ivanov, M. A., Zaeva, A. S., Philippova, T. S. & Antzutkin, O. N. (2011). *Inorg. Chim. Acta*, **368**, 263–270.
 Rohl, A. L., Moret, M., Kaminsky, W., Claborn, K., McKinnon, J. J. & Kahr, B. (2008). *Cryst. Growth Des.* **8**, 4517–4525.
 Sheldrick, G. M. (2008). *Acta Cryst.* **A64**, 112–122.
 Sheldrick, G. M. (2015). *Acta Cryst.* **C71**, 3–8.
 Sim, J.-H., Jamaludin, N. S., Khoo, C.-H., Cheah, Y.-K., Halim, S. N. B. A., Seng, H.-L. & Tiekink, E. R. T. (2014). *Gold Bull.* **47**, 225–236.
 Spackman, M. A., McKinnon, J. J. & Jayatilaka, D. (2008). *CrystEngComm*, **10**, 377–388.
 Suen, M.-C. & Wang, J.-C. (2007). *J. Coord. Chem.* **60**, 2197–2205.
 Suen, M.-C., Wang, Y.-H. & Wang, J.-C. (2004). *J. Chin. Chem. Soc. (Taipei)*, **51**, 43–48.
 Tan, Y. S., Halim, S. N. A. & Tiekink, E. R. T. (2016). *Z. Kristallogr.* **231** DOI: 10.1515/zkri-2015-1889.
 Tan, Y. S., Ooi, K. K., Ang, K. P., Akim, A. Md., Cheah, Y.-K., Halim, S. N. A., Seng, H.-L. & Tiekink, E. R. T. (2015). *J. Inorg. Biochem.* **150**, 48–62.
 Tan, Y. S., Sudlow, A. L., Molloy, K. C., Morishima, Y., Fujisawa, K., Jackson, W. J., Henderson, W., Halim, S. N. B. A., Ng, S. W. & Tiekink, E. R. T. (2013). *Cryst. Growth Des.* **13**, 3046–3056.
 Tiekink, E. R. T. (2003). *CrystEngComm*, **5**, 101–113.
 Wahab, N. A. A., Baba, I., Mohamed Tahir, M. I. & Tiekink, E. R. T. (2011). *Acta Cryst.* **E67**, m551–m552.
 Westrip, S. P. (2010). *J. Appl. Cryst.* **43**, 920–925.
 Wolff, S. K., Grimwood, D. J., McKinnon, J. J., Turner, M. J., Jayatilaka, D. & Spackman, M. A. (2012). *Crystal Explorer*. The University of Western Australia.
 Yu, J.-H., Ye, L., Bi, M.-H., Hou, Q., Zhang, X. & Xu, J.-Q. (2007). *Inorg. Chim. Acta*, **360**, 1987–1994.

supporting information

Acta Cryst. (2016). E72, 158-163 [doi:10.1107/S2056989016000165]

Bis[*N*-(2-hydroxyethyl)-*N*-isopropylthiocarbamate- κ^2 S,*S'*](piperazine- κ N)cadmium: crystal structure and Hirshfeld surface analysis

Siti Artikah M. Safbri, Siti Nadiah Abdul Halim, Mukesh M. Jotani and Edward R. T. Tiekink

Computing details

Data collection: *CrysAlis PRO* (Agilent, 2011); cell refinement: *CrysAlis PRO* (Agilent, 2011); data reduction: *CrysAlis PRO* (Agilent, 2011); program(s) used to solve structure: *SHELXS97* (Sheldrick, 2008); program(s) used to refine structure: *SHELXL2014/7* (Sheldrick, 2015); molecular graphics: *ORTEP-3 for Windows* (Farrugia, 2012) and *DIAMOND* (Brandenburg, 2006); software used to prepare material for publication: *publCIF* (Westrip, 2010).

Bis[*N*-(2-hydroxyethyl)-*N*-isopropylthiocarbamate- κ^2 S,*S'*](piperazine- κ N)cadmium

Crystal data

[Cd(C₆H₁₂NOS₂)₂(C₄H₁₀N₂)₂]

$M_r = 555.11$

Monoclinic, $P2_1/c$

$a = 15.341$ (3) Å

$b = 16.9915$ (7) Å

$c = 9.0308$ (8) Å

$\beta = 100.620$ (16)°

$V = 2313.7$ (5) Å³

$Z = 4$

$F(000) = 1144$

$D_x = 1.594$ Mg m⁻³

Mo $K\alpha$ radiation, $\lambda = 0.71073$ Å

Cell parameters from 7141 reflections

$\theta = 2.3$ – 27.5 °

$\mu = 1.32$ mm⁻¹

$T = 100$ K

Block, colourless

$0.35 \times 0.30 \times 0.25$ mm

Data collection

Agilent SuperNova Dual

diffractometer with Atlas detector

Radiation source: SuperNova (Mo) X-ray

Source

Mirror monochromator

Detector resolution: 10.4041 pixels mm⁻¹

ω scan

Absorption correction: multi-scan

(*CrysAlis PRO*; Agilent, 2011)

$T_{\min} = 0.805$, $T_{\max} = 1.000$

19918 measured reflections

5336 independent reflections

4483 reflections with $I > 2\sigma(I)$

$R_{\text{int}} = 0.035$

$\theta_{\text{max}} = 27.6$ °, $\theta_{\text{min}} = 2.6$ °

$h = -19 \rightarrow 19$

$k = -22 \rightarrow 21$

$l = -11 \rightarrow 11$

Refinement

Refinement on F^2

Least-squares matrix: full

$R[F^2 > 2\sigma(F^2)] = 0.026$

$wR(F^2) = 0.058$

$S = 1.03$

5336 reflections

260 parameters

4 restraints

Hydrogen site location: mixed

$w = 1/[\sigma^2(F_o^2) + (0.0205P)^2 + 0.8997P]$

where $P = (F_o^2 + 2F_c^2)/3$

$(\Delta/\sigma)_{\text{max}} = 0.001$

$\Delta\rho_{\text{max}} = 0.45$ e Å⁻³

$\Delta\rho_{\text{min}} = -0.45$ e Å⁻³

Special details

Geometry. All esds (except the esd in the dihedral angle between two l.s. planes) are estimated using the full covariance matrix. The cell esds are taken into account individually in the estimation of esds in distances, angles and torsion angles; correlations between esds in cell parameters are only used when they are defined by crystal symmetry. An approximate (isotropic) treatment of cell esds is used for estimating esds involving l.s. planes.

Fractional atomic coordinates and isotropic or equivalent isotropic displacement parameters (\AA^2)

	<i>x</i>	<i>y</i>	<i>z</i>	$U_{\text{iso}}^*/U_{\text{eq}}$
Cd	0.76764 (2)	0.52627 (2)	0.47410 (2)	0.01437 (5)
S1	0.78258 (4)	0.56986 (3)	0.74785 (6)	0.01975 (12)
S2	0.93633 (3)	0.55625 (3)	0.59115 (6)	0.01631 (12)
S3	0.74500 (4)	0.57217 (3)	0.20148 (6)	0.02150 (13)
S4	0.59316 (3)	0.56165 (3)	0.36324 (6)	0.01639 (12)
O1	1.18537 (10)	0.63462 (9)	0.85852 (17)	0.0188 (3)
H1O	1.2282 (12)	0.6228 (14)	0.923 (2)	0.028*
O2	0.33805 (10)	0.64272 (9)	0.05591 (18)	0.0198 (3)
H2O	0.3353 (17)	0.6586 (14)	0.1420 (15)	0.030*
N1	0.94525 (11)	0.62212 (10)	0.86113 (19)	0.0144 (4)
N2	0.58291 (11)	0.62440 (10)	0.0898 (2)	0.0146 (4)
N3	0.76459 (11)	0.39219 (10)	0.4310 (2)	0.0145 (4)
H3N	0.7843 (14)	0.3924 (13)	0.3467 (16)	0.017*
N4	0.69255 (12)	0.31320 (10)	0.6653 (2)	0.0178 (4)
H4N	0.6902 (15)	0.2653 (7)	0.631 (2)	0.021*
C1	0.89375 (14)	0.58600 (11)	0.7450 (2)	0.0139 (4)
C2	1.03323 (13)	0.65184 (12)	0.8466 (2)	0.0161 (4)
H2A	1.0464	0.6989	0.9115	0.019*
H2B	1.0309	0.6689	0.7411	0.019*
C3	1.10896 (13)	0.59392 (12)	0.8877 (3)	0.0177 (5)
H3A	1.1165	0.5789	0.9952	0.021*
H3B	1.0980	0.5458	0.8252	0.021*
C4	0.90981 (14)	0.64845 (13)	0.9957 (2)	0.0183 (5)
H4	0.8542	0.6181	0.9977	0.022*
C5	0.88517 (16)	0.73502 (14)	0.9818 (3)	0.0277 (6)
H5A	0.8426	0.7437	0.8881	0.042*
H5B	0.9386	0.7665	0.9806	0.042*
H5C	0.8584	0.7507	1.0678	0.042*
C6	0.97444 (15)	0.63025 (14)	1.1409 (3)	0.0255 (5)
H6A	0.9920	0.5748	1.1413	0.038*
H6B	0.9458	0.6407	1.2274	0.038*
H6C	1.0271	0.6636	1.1474	0.038*
C7	0.63461 (14)	0.58907 (11)	0.2067 (2)	0.0148 (4)
C8	0.49551 (13)	0.65624 (12)	0.1036 (2)	0.0156 (4)
H8A	0.4834	0.7030	0.0377	0.019*
H8B	0.4981	0.6741	0.2087	0.019*
C9	0.41828 (14)	0.59923 (12)	0.0634 (3)	0.0183 (5)
H9A	0.4198	0.5741	-0.0350	0.022*
H9B	0.4222	0.5575	0.1408	0.022*

C10	0.61846 (14)	0.64931 (12)	-0.0452 (2)	0.0173 (5)
H10	0.6722	0.6166	-0.0493	0.021*
C11	0.64800 (16)	0.73483 (13)	-0.0293 (3)	0.0253 (5)
H11A	0.6902	0.7417	0.0654	0.038*
H11B	0.5963	0.7687	-0.0292	0.038*
H11C	0.6766	0.7492	-0.1140	0.038*
C12	0.55260 (15)	0.63515 (13)	-0.1906 (3)	0.0230 (5)
H12A	0.5319	0.5805	-0.1936	0.034*
H12B	0.5815	0.6451	-0.2769	0.034*
H12C	0.5019	0.6707	-0.1950	0.034*
C13	0.67256 (14)	0.36241 (12)	0.4019 (2)	0.0163 (4)
H13A	0.6711	0.3086	0.3594	0.020*
H13B	0.6349	0.3967	0.3277	0.020*
C14	0.63728 (14)	0.36126 (12)	0.5478 (2)	0.0173 (5)
H14A	0.6347	0.4158	0.5851	0.021*
H14B	0.5761	0.3400	0.5281	0.021*
C15	0.78608 (14)	0.33777 (13)	0.6863 (2)	0.0187 (5)
H15A	0.8225	0.3006	0.7562	0.022*
H15B	0.7921	0.3905	0.7338	0.022*
C16	0.82184 (14)	0.34096 (12)	0.5409 (2)	0.0180 (5)
H16A	0.8831	0.3619	0.5610	0.022*
H16B	0.8234	0.2873	0.4988	0.022*

Atomic displacement parameters (\AA^2)

	U^{11}	U^{22}	U^{33}	U^{12}	U^{13}	U^{23}
Cd	0.01554 (9)	0.01362 (8)	0.01268 (9)	-0.00077 (6)	-0.00071 (6)	0.00017 (6)
S1	0.0124 (3)	0.0291 (3)	0.0181 (3)	-0.0043 (2)	0.0038 (2)	-0.0087 (2)
S2	0.0142 (3)	0.0209 (3)	0.0139 (3)	0.0001 (2)	0.0027 (2)	-0.0039 (2)
S3	0.0130 (3)	0.0336 (3)	0.0182 (3)	0.0052 (2)	0.0036 (2)	0.0104 (2)
S4	0.0155 (3)	0.0184 (3)	0.0156 (3)	0.0017 (2)	0.0038 (2)	0.0025 (2)
O1	0.0119 (8)	0.0277 (8)	0.0162 (8)	-0.0023 (6)	0.0008 (6)	0.0011 (7)
O2	0.0132 (8)	0.0279 (9)	0.0177 (8)	0.0031 (6)	0.0011 (7)	-0.0014 (7)
N1	0.0130 (9)	0.0167 (9)	0.0142 (9)	-0.0016 (7)	0.0042 (7)	-0.0024 (7)
N2	0.0121 (9)	0.0155 (9)	0.0159 (9)	0.0026 (7)	0.0014 (7)	0.0016 (7)
N3	0.0145 (9)	0.0171 (9)	0.0123 (9)	0.0004 (7)	0.0035 (7)	0.0018 (7)
N4	0.0212 (10)	0.0138 (9)	0.0186 (10)	-0.0017 (7)	0.0045 (8)	0.0013 (7)
C1	0.0150 (11)	0.0109 (10)	0.0152 (11)	0.0019 (8)	0.0015 (8)	0.0023 (8)
C2	0.0135 (11)	0.0188 (11)	0.0161 (11)	-0.0049 (8)	0.0026 (9)	-0.0011 (9)
C3	0.0134 (11)	0.0214 (11)	0.0175 (11)	-0.0026 (8)	0.0010 (9)	0.0003 (9)
C4	0.0154 (11)	0.0246 (12)	0.0157 (11)	-0.0044 (9)	0.0050 (9)	-0.0069 (9)
C5	0.0265 (13)	0.0304 (13)	0.0271 (14)	0.0040 (10)	0.0070 (11)	-0.0108 (11)
C6	0.0230 (13)	0.0384 (14)	0.0157 (12)	-0.0078 (10)	0.0050 (10)	-0.0040 (10)
C7	0.0146 (11)	0.0122 (10)	0.0170 (11)	-0.0007 (8)	0.0014 (9)	-0.0008 (8)
C8	0.0153 (11)	0.0138 (10)	0.0176 (11)	0.0026 (8)	0.0027 (9)	0.0011 (8)
C9	0.0151 (11)	0.0205 (11)	0.0192 (12)	0.0026 (8)	0.0027 (9)	0.0003 (9)
C10	0.0145 (11)	0.0220 (11)	0.0153 (11)	0.0028 (8)	0.0026 (9)	0.0050 (9)
C11	0.0255 (13)	0.0265 (13)	0.0231 (13)	-0.0060 (10)	0.0025 (10)	0.0072 (10)

C12	0.0210 (12)	0.0279 (12)	0.0184 (12)	0.0024 (9)	-0.0004 (10)	0.0031 (10)
C13	0.0167 (11)	0.0151 (10)	0.0160 (11)	-0.0013 (8)	0.0000 (9)	-0.0019 (8)
C14	0.0145 (11)	0.0159 (10)	0.0209 (12)	-0.0009 (8)	0.0016 (9)	0.0000 (9)
C15	0.0181 (11)	0.0197 (11)	0.0173 (12)	0.0040 (9)	0.0008 (9)	0.0052 (9)
C16	0.0157 (11)	0.0175 (11)	0.0203 (12)	0.0031 (8)	0.0023 (9)	0.0020 (9)

Geometric parameters (Å, °)

Cd—S1	2.5503 (6)	C4—H4	1.0000
Cd—S2	2.6580 (8)	C5—H5A	0.9800
Cd—S3	2.5446 (6)	C5—H5B	0.9800
Cd—S4	2.7461 (8)	C5—H5C	0.9800
Cd—N3	2.3102 (17)	C6—H6A	0.9800
C1—S1	1.732 (2)	C6—H6B	0.9800
C1—S2	1.717 (2)	C6—H6C	0.9800
C7—S3	1.727 (2)	C8—C9	1.522 (3)
C7—S4	1.718 (2)	C8—H8A	0.9900
O1—C3	1.427 (2)	C8—H8B	0.9900
O1—H1O	0.821 (10)	C9—H9A	0.9900
O2—C9	1.426 (2)	C9—H9B	0.9900
O2—H2O	0.831 (10)	C10—C12	1.521 (3)
N1—C1	1.340 (3)	C10—C11	1.521 (3)
N1—C2	1.470 (3)	C10—H10	1.0000
N1—C4	1.488 (3)	C11—H11A	0.9800
N2—C7	1.340 (3)	C11—H11B	0.9800
N2—C8	1.472 (3)	C11—H11C	0.9800
N2—C10	1.487 (3)	C12—H12A	0.9800
N3—C13	1.477 (3)	C12—H12B	0.9800
N3—C16	1.481 (3)	C12—H12C	0.9800
N3—H3N	0.869 (9)	C13—C14	1.514 (3)
N4—C15	1.473 (3)	C13—H13A	0.9900
N4—C14	1.477 (3)	C13—H13B	0.9900
N4—H4N	0.868 (9)	C14—H14A	0.9900
C2—C3	1.516 (3)	C14—H14B	0.9900
C2—H2A	0.9900	C15—C16	1.515 (3)
C2—H2B	0.9900	C15—H15A	0.9900
C3—H3A	0.9900	C15—H15B	0.9900
C3—H3B	0.9900	C16—H16A	0.9900
C4—C5	1.518 (3)	C16—H16B	0.9900
C4—C6	1.523 (3)		
S1—Cd—S2	69.63 (2)	C4—C6—H6C	109.5
S1—Cd—S3	145.16 (2)	H6A—C6—H6C	109.5
S1—Cd—S4	101.38 (2)	H6B—C6—H6C	109.5
S1—Cd—N3	116.43 (5)	N2—C7—S4	120.98 (16)
S2—Cd—S3	105.98 (2)	N2—C7—S3	119.60 (16)
S2—Cd—S4	156.230 (18)	S4—C7—S3	119.42 (12)
S2—Cd—N3	104.12 (4)	N2—C8—C9	115.29 (17)

S3—Cd—S4	68.29 (2)	N2—C8—H8A	108.5
S3—Cd—N3	98.30 (5)	C9—C8—H8A	108.5
S4—Cd—N3	99.57 (4)	N2—C8—H8B	108.5
C1—S1—Cd	86.81 (7)	C9—C8—H8B	108.5
C1—S2—Cd	83.72 (7)	H8A—C8—H8B	107.5
C7—S3—Cd	89.09 (8)	O2—C9—C8	107.97 (17)
C7—S4—Cd	82.85 (7)	O2—C9—H9A	110.1
C3—O1—H1O	109.0 (18)	C8—C9—H9A	110.1
C9—O2—H2O	108.4 (18)	O2—C9—H9B	110.1
C1—N1—C2	120.42 (18)	C8—C9—H9B	110.1
C1—N1—C4	121.68 (17)	H9A—C9—H9B	108.4
C2—N1—C4	116.70 (16)	N2—C10—C12	112.18 (18)
C7—N2—C8	120.95 (18)	N2—C10—C11	110.04 (18)
C7—N2—C10	121.38 (17)	C12—C10—C11	111.81 (18)
C8—N2—C10	116.24 (16)	N2—C10—H10	107.5
C13—N3—C16	110.33 (16)	C12—C10—H10	107.5
C13—N3—Cd	110.91 (12)	C11—C10—H10	107.5
C16—N3—Cd	118.40 (13)	C10—C11—H11A	109.5
C13—N3—H3N	108.7 (15)	C10—C11—H11B	109.5
C16—N3—H3N	109.3 (15)	H11A—C11—H11B	109.5
Cd—N3—H3N	98.3 (15)	C10—C11—H11C	109.5
C15—N4—C14	110.64 (16)	H11A—C11—H11C	109.5
C15—N4—H4N	106.7 (16)	H11B—C11—H11C	109.5
C14—N4—H4N	106.4 (15)	C10—C12—H12A	109.5
N1—C1—S2	120.73 (16)	C10—C12—H12B	109.5
N1—C1—S1	120.06 (16)	H12A—C12—H12B	109.5
S2—C1—S1	119.20 (12)	C10—C12—H12C	109.5
N1—C2—C3	115.48 (17)	H12A—C12—H12C	109.5
N1—C2—H2A	108.4	H12B—C12—H12C	109.5
C3—C2—H2A	108.4	N3—C13—C14	109.43 (17)
N1—C2—H2B	108.4	N3—C13—H13A	109.8
C3—C2—H2B	108.4	C14—C13—H13A	109.8
H2A—C2—H2B	107.5	N3—C13—H13B	109.8
O1—C3—C2	105.00 (16)	C14—C13—H13B	109.8
O1—C3—H3A	110.7	H13A—C13—H13B	108.2
C2—C3—H3A	110.7	N4—C14—C13	112.50 (18)
O1—C3—H3B	110.7	N4—C14—H14A	109.1
C2—C3—H3B	110.7	C13—C14—H14A	109.1
H3A—C3—H3B	108.8	N4—C14—H14B	109.1
N1—C4—C5	110.29 (18)	C13—C14—H14B	109.1
N1—C4—C6	111.36 (17)	H14A—C14—H14B	107.8
C5—C4—C6	112.35 (18)	N4—C15—C16	113.49 (18)
N1—C4—H4	107.5	N4—C15—H15A	108.9
C5—C4—H4	107.5	C16—C15—H15A	108.9
C6—C4—H4	107.5	N4—C15—H15B	108.9
C4—C5—H5A	109.5	C16—C15—H15B	108.9
C4—C5—H5B	109.5	H15A—C15—H15B	107.7
H5A—C5—H5B	109.5	N3—C16—C15	109.71 (17)

C4—C5—H5C	109.5	N3—C16—H16A	109.7
H5A—C5—H5C	109.5	C15—C16—H16A	109.7
H5B—C5—H5C	109.5	N3—C16—H16B	109.7
C4—C6—H6A	109.5	C15—C16—H16B	109.7
C4—C6—H6B	109.5	H16A—C16—H16B	108.2
H6A—C6—H6B	109.5		
C2—N1—C1—S2	12.9 (2)	Cd—S4—C7—N2	-173.40 (17)
C4—N1—C1—S2	179.99 (15)	Cd—S4—C7—S3	5.59 (11)
C2—N1—C1—S1	-166.32 (14)	Cd—S3—C7—N2	173.01 (16)
C4—N1—C1—S1	0.8 (3)	Cd—S3—C7—S4	-5.99 (11)
Cd—S2—C1—N1	-171.64 (16)	C7—N2—C8—C9	-90.4 (2)
Cd—S2—C1—S1	7.59 (11)	C10—N2—C8—C9	103.1 (2)
Cd—S1—C1—N1	171.36 (16)	N2—C8—C9—O2	-169.59 (17)
Cd—S1—C1—S2	-7.88 (11)	C7—N2—C10—C12	141.10 (19)
C1—N1—C2—C3	-89.4 (2)	C8—N2—C10—C12	-52.4 (2)
C4—N1—C2—C3	102.9 (2)	C7—N2—C10—C11	-93.8 (2)
N1—C2—C3—O1	177.54 (16)	C8—N2—C10—C11	72.7 (2)
C1—N1—C4—C5	-96.9 (2)	C16—N3—C13—C14	59.9 (2)
C2—N1—C4—C5	70.7 (2)	Cd—N3—C13—C14	-73.30 (17)
C1—N1—C4—C6	137.7 (2)	C15—N4—C14—C13	52.8 (2)
C2—N1—C4—C6	-54.8 (2)	N3—C13—C14—N4	-57.4 (2)
C8—N2—C7—S4	13.3 (3)	C14—N4—C15—C16	-51.7 (2)
C10—N2—C7—S4	179.18 (14)	C13—N3—C16—C15	-58.4 (2)
C8—N2—C7—S3	-165.65 (14)	Cd—N3—C16—C15	70.83 (19)
C10—N2—C7—S3	0.2 (3)	N4—C15—C16—N3	54.8 (2)

Hydrogen-bond geometry (\AA , $^\circ$)

<i>D</i> —H \cdots <i>A</i>	<i>D</i> —H	H \cdots <i>A</i>	<i>D</i> \cdots <i>A</i>	<i>D</i> —H \cdots <i>A</i>
O1—H1O \cdots O2 ⁱ	0.82 (2)	1.91 (2)	2.673 (2)	155 (2)
O2—H2O \cdots N4 ⁱⁱ	0.83 (2)	1.93 (2)	2.749 (2)	169 (3)
N3—H3N \cdots O1 ⁱⁱⁱ	0.87 (2)	2.05 (2)	2.894 (2)	165 (2)
N4—H4N \cdots O2 ^{iv}	0.87 (1)	2.67 (1)	3.501 (3)	162 (1)
C4—H4 \cdots S3 ^v	1.00	2.82	3.641 (3)	140
C10—H10 \cdots S1 ^{vi}	1.00	2.83	3.659 (3)	141

Symmetry codes: (i) $x+1, y, z+1$; (ii) $-x+1, -y+1, -z+1$; (iii) $-x+2, -y+1, -z+1$; (iv) $-x+1, y-1/2, -z+1/2$; (v) $x, y, z+1$; (vi) $x, y, z-1$.